



Comparing Bayesian and traditional end-member mixing approaches for hydrograph separation in a glacierized basin

Zhihua He^{1,2}, Katy Unger-Shayesteh³, Sergiy Vorogushyn¹, Stephan M. Weise⁴, Doris Duethmann⁵, Olga
Kalashnikova⁶, Abror Gafurov¹, Bruno Merz^{1,2}

¹GFZ German Research Centre for Geosciences, Section Hydrology, Telegrafenberg, Potsdam,
Germany.

²University of Potsdam, Institute for Environmental Sciences and Geography, Potsdam, Germany

³Now at German Aerospace Center (DLR), International Relations, Linder Höhe, Cologne, Germany

⁴UFZ Helmholtz Centre for Environmental Research UFZ, Department Catchment Hydrology, Halle
Germany

⁵Institute of Hydraulic Engineering and Water Resources Management, Vienna University of
Technology (TU Wien), Vienna, Austria

⁶CAIAG Central Asian Institute of Applied Geosciences, Department Climate, Water and Natural
Resources, Bishkek, Kyrgyzstan

^{*}Now at Centre for Hydrology, University of Saskatchewan, Saskatoon, Saskatchewan, Canada



28 Abstract

29 Water tracer data have been successfully used for hydrograph separation in glacierized
30 basins. However, uncertainties in the hydrograph separation are large in these basins, caused
31 by the spatio-temporal variability in the tracer signatures of water sources, the uncertainty of
32 water sampling and the mixing model uncertainty. In this study, we used electrical conductivity
33 (EC) measurements and two isotope signatures ($\delta^{18}\text{O}$ and $\delta^2\text{H}$) to label the runoff components,
34 including groundwater, snow and glacier meltwater, and rainfall, in a Central Asia glacierized
35 basin. The contributions of runoff components (CRC) to the total runoff, as well as the
36 corresponding uncertainty, were quantified by two mixing approaches: a traditional end-
37 member mixing approach (TEMMA) and a Bayesian end-member mixing approach. The
38 performance of the two mixing approaches were compared in three seasons, distinguished as
39 cold season, snowmelt season and glacier melt season. Results show that: 1) The Bayesian
40 approach generally estimated smaller uncertainty ranges for the CRC compared to the TEMMA.
41 2) The Bayesian approach tended to be less sensitive to the sampling uncertainties of meltwater
42 than the TEMMA. 3) Ignoring the model uncertainty caused by the isotope fractionation likely
43 led to an overestimated rainfall contribution and an underestimated meltwater share in the
44 melt seasons. Our study provides the first comparison of the two end-member mixing
45 approaches for hydrograph separation in glacierized basins, and gives insights for the
46 application of tracer-based mixing approaches for similar basins.



1. Introduction

Glaciers and snowpack store a large amount of fresh water in glacierized basins, thus providing an important water source for downstream human societies and ecosystems (Barnett et al., 2005; Viviroli et al., 2007; He et al., 2014; Penna et al., 2016). Seasonal meltwater and rainfall play significant roles in shaping the magnitude and timing of runoff in these basins (Rahman et al., 2015; Pohl et al., 2017). Quantifying the seasonal contributions of the runoff components (CRC), including groundwater, snowmelt, glacier melt and rainfall, to the total runoff is therefore highly needed for the understanding of the dynamics of water resource in glacierized basins under the current climate warming (La Frenierre and Mark, 2014; Penna et al., 2014; He et al., 2015).

The traditional end-member mixing approach (TEMMA) has been widely used for hydrograph separation in glacierized basins across the world (Dahlke et al., 2014; Sun et al., 2016a; Pu et al., 2017). For instance, studies in the Italian glacierized Alpine catchments indicate the successful application of the TEMMA to estimate the proportions of groundwater, snow and glacier meltwater based on water stable isotopes and EC (e.g., Chiogna et al. 2014, Engel et al. 2016 and Penna et al. 2017). Li et al. (2014) confirmed significant contributions of snow and glacier melt runoff to total runoff in the Qilian Mountains using TEMMA. Maurya et al. (2011) reported the contribution of glacial ice meltwater to the total runoff in a Himalayan basin on $\delta^{18}\text{O}$ and EC, using a three-component TEMMA.

However, difficulties in field sampling and seasonal inaccessibility often limit the application of TEMMA in high-elevation glacierized basins (Rahman et al., 2015). Moreover, uncertainties for the CRC quantified by the TEMMA are typically high (Klaus and McDonnell, 2013), which can be caused by statistical uncertainty and model uncertainty. Statistical uncertainty refers to the spatio-temporal variability for the tracer signature sampling uncertainty and laboratory measurement error (Joerin et al., 2002). Model uncertainty is determined by the assumptions of the TEMMA, which might not agree with reality (Joerin et al., 2002; Klaus and McDonnell, 2013). For example, the fractionation effect on isotope ratios caused by evaporation during the mixing process can result in significant errors given the constant tracer assumption in the TEMMA (Moore and Semmens, 2008).

The Gaussian error propagation technique has been typically applied along with TEMMA to estimate the uncertainty for the hydrograph separation, assuming the uncertainty associated with each source is independent from the uncertainty of other sources (Genereux, 1998; Pu et al., 2013). The spatio-temporal variability for the tracer signatures is estimated by multiplying the t values of the Student's t distribution at the selected significance level with the



81 standard deviations (Sd) of the measured tracer signatures (Pu et al., 2013; Penna et al., 2016;
 82 Sun et al., 2016b). Although this approach has been successfully used in various glacierized
 83 basins, some recurring issues remain. These include (1) inappropriate estimation of the
 84 variability of tracer signatures of water sources when only few water samples are available
 85 (Dahlke et al., 2014), and (2) negligence of the correlation of water tracers and runoff
 86 components caused by the assumption of independence of the uncertainty sources. Further, the
 87 model uncertainty caused by the fractionation effect on isotope ratios during the mixing process
 88 is also often ignored.

89 The Bayesian end-member mixing approach (abbreviated as Bayesian approach) shows
 90 the potential to estimate the proportions of individual components to the mixing variable in a
 91 more rigorous statistical way (Parnell et al., 2010). For hydrograph separation, the water tracer
 92 signatures of the water sources are first assumed to obey specific prior distributions. Their
 93 posterior distribution are then obtained by updating the prior distributions with the observation
 94 likelihood derived from water samples. In the last step, the CRC to the total runoff are estimated
 95 based on the balance of the posterior water tracer signatures. The distributions, expressing the
 96 uncertainties for the CRC and parameters, are typically estimated in a Markov Chain Monte
 97 Carlo (MCMC) procedure.

98 Although the Bayesian approach can be applied in cases when the sample sizes are
 99 small (Ward et al., 2010), it has been rarely used for hydrograph separation in glacierized basins.
 100 To the authors' knowledge, there have been only three studies, including Brown et al. (2006),
 101 who conducted the hydrograph separation in a glacierized basin in the French Pyrenees using a
 102 three-component Bayesian approach. Further, Cable et al. (2011) quantified the CRC to total
 103 runoff in a glacierized basin in the American Rocky Mountains. They used a hierarchical
 104 Bayesian framework to incorporate temporal and spatial variability in the water isotope data
 105 into the mixing model. Recently, Beria et al. (2019) used a classic Bayesian approach to
 106 estimate the uncertainty for the CRC in a Swiss alpine catchment. However, the performance
 107 of the Bayesian approach has not been compared to the TEMMA. Moreover, the sensitivity of
 108 the Bayesian approach to the water sampling uncertainty is still not clear. The potential of the
 109 Bayesian approach to estimate the fractionation effect on isotopic signatures during the mixing
 110 process has not been investigated either.

111 In this study, we compare TEMMA and the Bayesian approach for hydrograph
 112 separation in a Central Asia glacierized basin, using water isotope and EC measurements. The
 113 research questions are: 1) How do TEMMA and the Bayesian approaches compare with respect
 114 to the quantification for the CRC? 2) What is the influence of the different uncertainty sources



(including variability of the tracer signatures, sampling uncertainty, and model uncertainty) on the estimated CRC in the two mixing approaches?

The paper is organized as follows: details on the study basin and water sampling are introduced in Section 2; assumptions of the two mixing approaches are described in Section 3; Section 4 estimates the CRC, as well as the corresponding uncertainties; discussion and conclusion finalize the paper in Sections 5 and 6, respectively.

2. Study area and data

2.1 Study area

Located in Kyrgyzstan, Central Asia, the Ala-Archa basin drains an area of 233 km², (Fig. 1), and glacier covers around 17% of the basin area. The elevation of the study basin extends from 1560 m to 4864 m a.s.l.. The seasonal dynamics of runoff in the river play an important role in the water availability for downstream agricultural irrigation. The generation of snow and glacier melt runoff generally show the largest effect on the runoff seasonality (Aizen et al., 2000; Aizen et al., 2007). In particular, the snowmelt runoff mainly occurs in the warm period from early March to middle September, and the glacier melt typically generates from the high-elevation areas during July to September (Aizen et al., 1996; He et al., 2018; He et al., 2019). We subsequently defined three runoff generation seasons as follows. Cold season: from October to February, in which the streamflow is fed mainly by groundwater and to a smaller extent by snowmelt and rainfall; Snowmelt season: from March to June, in which the streamflow is fed chiefly by snowmelt and groundwater and additionally by rainfall; Glacier melt season: from July to September, in which the streamflow is fed by significant glacier melt and groundwater, rainfall and snowmelt.

Two meteorological stations (Fig. 1), i.e., Alplager (at elevation of 2100 m a.s.l.) and Baitik (at elevation of 1580 m a.s.l.), have been set up in the basin since 1960s to collect daily precipitation and temperature data. The Ala-Archa hydrological station has been set up at the same site of the Baitik meteorological station to collect daily average discharge data since 1960s. The dynamics of glacier mass balance and snow mass balance in the accumulation zone have been surveyed in summer field campaigns through 2012-2017.

2.2 Water transport data

Since July of 2013, stream water samples have been collected weekly by local station operators, from the river channel close to the Alplager and Baitik meteorological sites, using pure plastic bottles (He et al., 2019). The sampling time slightly varied around noon every Wednesday. Precipitation samples were collected during 2012-2017 at four sites across the basin (Fig. 1). At the Alplager and Baitik meteorological sites, the precipitation samples were



first collected from fixed rain collectors (immediately after the rainfall/snowfall events), and then accumulated in two indoor rain containers over one month. The mixed water in the containers were then sampled for isotopic analysis every month. The indoor rain containers were filled with thin mineral oil layers for monthly precipitation accumulation and stored in cold places. Additionally, two plastic rain collectors PALMEX, specifically designed for isotopic sampling to prevent evaporation, were set up at the elevations of 2580 m a.s.l. and 3300 m a.s.l. to collect precipitation in high-elevation areas (Fig. 1). Precipitation samples were collected monthly from these two rain collectors during the period from May to October when the high-elevation areas were accessible.

Glacier meltwater were sampled during the summer field campaigns in each year of 2012-2017. Samples of meltwater flowing on the Golubin glacier in the ablation zone and at the glacier tongue were collected by pure plastic bottles and then stored in a cooling box (Fig. 1, the elevation of the sampling sites ranges from 3280 m to 3805 m a.s.l.). Snow samples were collected through early March to early October during 2012-2017, as the sampling sites are generally not accessible caused by the heavy snow accumulation in the remaining months. The elevation of the multiple snow sampling sites ranges from 1580 m to 4050 m a.s.l. (Fig. 1). The whole snow profile at each sampling site was collected through drilling a 1.2 m pure plastic tube into the snowpack. The snow in the whole tube were then collected by plastic bags and stored in a cooling box. After all the snow in the plastic bags melted out, the mixed snow meltwater were then sampled by pure plastic bottles. Groundwater samples were also collected through March to October during 2012-2017, from a spring draining to the river (Fig. 1, 2400 m a.s.l.) using pure plastic bottles. The spring is located at the foot of a rocky hill, around 60 meters away from the river channel.

All samples were stored at 4 °C and then delivered to the laboratory of Helmholtz Center for Environmental Research (UFZ) in Halle of Germany by flight. Isotopic compositions of water samples were measured using a Laser-based infrared spectrometry (LGR TIWA 45, Picarro L2-i). The measurement precisions of $\delta^{18}\text{O}$ and $\delta^2\text{H}$ are: $\pm 0.25\text{‰}$ and $\pm 0.4\text{‰}$, respectively, after the calibration against the common VSMOW standard. EC values of the water samples were measured using portable PH/TDS/EC meters. Abnormal isotopic compositions caused by obvious evaporation and abnormal EC values caused by impurities were discarded.

3. Methodology

The hydrograph separation is carried out in each of the three seasons (i.e., cold season, snowmelt season and glacier melt season). Water samples collected in the period from 2012 to



2017 are distributed into each of the three seasons for the hydrograph separation. The CRC estimated by the mixing approaches refer to the mean contributions in each of the three seasons during the period of 2012-2017, i.e., the inter-annual variability of CRC were not considered. The mixing approaches applied for the hydrograph separation in each season are summarized in Table 2.

3.1 Traditional end-member mixing approach (TEMMA)

The main assumptions of TEMMA are as follows (Kong and Pang, 2012): (1) The water tracer signature of each runoff component is constant during the analyzed period; (2) The water tracer signatures of the runoff components are significantly different from each other; (3) Water tracer signatures are conservative in the mixing process. In the cold and snowmelt seasons, a three-component TEMMA method (TEMMA_3, Table 2) is used. Since the precision of $\delta^{18}\text{O}$ (± 0.25 ‰) measured in the lab is higher than that of $\delta^2\text{H}$ (± 0.4 ‰) and both are strongly correlated, the TEMMA_3 is based on $\delta^{18}\text{O}$ and EC. In the glacier melt season, both the TEMMA_3 and the four-component TEMMA (TEMMA_4, Table 2) are used. In the TEMMA_3, glacier melt and snowmelt are assumed as one end-member, considering their similar tracer signatures. In the TEMMA_4, glacier melt and snowmelt are treated as two end-members separately, and $\delta^{18}\text{O}$ and $\delta^2\text{H}$ are used as two separate tracers. The following equations (Eqs. 1-5) are used to estimate CRC (f_{1-3}) and the corresponding uncertainty in the TEMMA_3 (Genereux, 1998).

$$\begin{cases} 1 = f_1 + f_2 + f_3, & \text{for water balance} \\ A = A_1 \cdot f_1 + A_2 \cdot f_2 + A_3 \cdot f_3, & \text{for water tracer A} \\ B = B_1 \cdot f_1 + B_2 \cdot f_2 + B_3 \cdot f_3, & \text{for water tracer B} \end{cases} \quad (1)$$

$$f_1 = \frac{AB_2 - AB_3 + A_2B_3 - A_2B + A_3B - A_3B_2}{A_1B_2 - A_1B_3 + A_2B_3 - A_2B_1 + A_3B_1 - A_3B_2} \quad (2)$$

$$f_2 = \frac{AB_3 - AB_1 + A_1B - A_1B_3 + A_3B_1 - A_3B}{A_1B_2 - A_1B_3 + A_2B_3 - A_2B_1 + A_3B_1 - A_3B_2} \quad (3)$$

$$f_3 = \frac{AB_1 - AB_2 + A_1B_2 - A_1B + A_2B - A_2B_1}{A_1B_2 - A_1B_3 + A_2B_3 - A_2B_1 + A_3B_1 - A_3B_2} \quad (4)$$

where the subscripts 1-3 refer to the three runoff components (i.e., groundwater, snowmelt/meltwater and rainfall), and A_1 - A_3 (B_1 - B_3) refers to the mean $\delta^{18}\text{O}$ (EC) values of runoff components. A and B stand for the mean $\delta^{18}\text{O}$ and EC values of the stream water. The mean isotope and EC values of precipitation are calculated as the monthly precipitation weighted average values. Similarly, the mean isotope and EC values of stream water are calculated as the weekly streamflow weighted average values.



Assuming the uncertainty of each variable is independent from the uncertainty in others, the Gaussian error propagation technique is applied to estimate the uncertainty of the CRC (f_{i-3}) using the following equation (Genereux, 1998):

$$W_{f_i} = \sqrt{\left(\frac{\partial f_i}{\partial A_1} W_{A_1}\right)^2 + \left(\frac{\partial f_i}{\partial A_2} W_{A_2}\right)^2 + \left(\frac{\partial f_i}{\partial A_3} W_{A_3}\right)^2 + \left(\frac{\partial f_i}{\partial A} W_A\right)^2 + \left(\frac{\partial f_i}{\partial B_1} W_{B_1}\right)^2 + \left(\frac{\partial f_i}{\partial B_2} W_{B_2}\right)^2 + \left(\frac{\partial f_i}{\partial B_3} W_{B_3}\right)^2 + \left(\frac{\partial f_i}{\partial B} W_B\right)^2} \quad (5)$$

where f_i stands for the contribution of a specific runoff component, and W is the uncertainty in the variable specified by the subscript. For the uncertainty of water tracer signatures (W_{A_i} and W_{B_i}), we multiply the Sd values of the measured tracer signatures with t values from the Student's t value table at the confidence level of 95%. The degree of freedom for the Student's t distribution is estimated as the number of water sample for each water source minus one. Analytical measurement errors are not considered in this approach, which, however, are minor compared to the uncertainty generated from water tracer variations (Penna et al., 2017; Pu et al., 2017). The *lsqnonneg* function in Matlab is used to solve Eqs. 1-4, which solves the equations in a least squares sense, given the constraint that the solution vector f has nonnegative elements. The TEMMA_4 uses the equations similar to Eqs. 1-5.

3.2 Bayesian mixing approach

The Bayesian approaches applied for each season are summarized in Table 2. Similar to the TEMMA, we apply a three-component Bayesian approach to all seasons, and additionally a four-component Bayesian approach in the glacier melt season. The three-component Bayesian approach has two types: the Bayesian_3_Cor approach considers the correlation between $\delta^{18}\text{O}$ and $\delta^2\text{H}$, whereas the Bayesian_3 approach assumes independence. The four-component Bayesian approach also has two types: Bayesian_4_Cor considering the correlation, and Bayesian_4 assuming independence between $\delta^{18}\text{O}$ and $\delta^2\text{H}$. The prior assumptions for the Bayesian approaches are listed as follows (similarly to Cable et al. 2011): In approaches considering the correlation between $\delta^{18}\text{O}$ and $\delta^2\text{H}$, the prior distributions of $\delta^{18}\text{O}$ and $\delta^2\text{H}$ of runoff components and stream water are assumed as bivariate normal distributions with means and precision matrix as $\mu^{18}\text{O}$, $\mu^2\text{H}$ and $\mathbf{\Omega}$, respectively (Eq. 6a). The precision matrix ($\mathbf{\Omega}$, i.e. the inverse of the covariance matrix) for the two isotopes is assumed as Wishart prior (Eq. 6b). When assuming independence between $\delta^{18}\text{O}$ and $\delta^2\text{H}$, the prior distributions of $\delta^{18}\text{O}$ ($\delta^2\text{H}$) of runoff components and stream water are assumed as normal distributions with means and variance of $\mu^{18}\text{O}$ and $\lambda^{18}\text{O}$ ($\mu^2\text{H}$ and $\lambda^2\text{H}$, Eqs. 6c-d). The mean values of the isotopes of runoff components (i.e., $\mu^{18}\text{O}$ and $\mu^2\text{H}$) are further estimated by independent normal priors (Eq. 7, Cable et al. 2011), which is assumed to consider the spatial variability of $\mu^{18}\text{O}$ and $\mu^2\text{H}$.



$$\begin{aligned}
 & \begin{cases} \begin{bmatrix} \delta^{18}O \\ \delta^2H \end{bmatrix} \sim \text{Multi_normal} \left(\begin{bmatrix} \mu^{18}O \\ \mu^2H \end{bmatrix}, \Omega \right) \end{cases} & (6a) \\
 & \begin{cases} \Omega \sim \text{Wishart} (2, \mathbf{V}) \end{cases} & (6b) \\
 & \begin{cases} \delta^{18}O \sim \text{Normal} (\mu^{18}O, \lambda^{18}O) \end{cases} & (6c) \\
 & \begin{cases} \delta^2H \sim \text{Normal} (\mu^2H, \lambda^2H) \end{cases} & (6d) \\
 & \begin{cases} \mu^{18}O \sim \text{Normal} (\gamma^{18}O, \sigma^{18}O) \end{cases} & (7a) \\
 & \begin{cases} \mu^2H \sim \text{Normal} (\gamma^2H, \sigma^2H) \end{cases} & (7b)
 \end{aligned}$$

where, $\lambda^{18}O$, $\gamma^{18}O$ and $\sigma^{18}O$ (λ^2H , γ^2H and σ^2H) are parameters used to describe the normal priors of $\delta^{18}O$ and $\mu^{18}O$ (δ^2H and μ^2H , see Table 3), which are estimated by likelihood observations (Table 3). \mathbf{V} is a 2*2 unit positive-definite matrix, and ‘2’ stands for the degree of freedom in the Wishart prior distribution.

The priors of EC values of runoff components and stream water are assumed as normal distributions (Eq. 8a), with mean ε and variance τ . Similarly, the spatial variability of the mean EC values of runoff components (ε) are assumed to follow a normal distribution with mean θ and variance ω (Eq. 8b). τ , θ and ω are parameters estimated by likelihood observations (Table 3).

$$\begin{aligned}
 & \begin{cases} EC \sim \text{Normal} (\varepsilon, \tau) \end{cases} & (8a) \\
 & \begin{cases} \varepsilon \sim \text{Normal} (\theta, \omega) \end{cases} & (8b) \\
 & \begin{cases} \begin{bmatrix} \mu^{18}O \\ \mu^2H \\ \varepsilon \end{bmatrix}_{\text{stream water}} = \sum_{i=1}^N f_i \cdot \begin{bmatrix} \mu^{18}O \\ \mu^2H \\ \varepsilon \end{bmatrix}_{\text{runoff component } i} \end{cases} & (9a) \\
 & \begin{cases} \mathbf{f} \sim \text{Dirichlet}(\boldsymbol{\alpha}) \end{cases} & (9b) \\
 & \begin{cases} \boldsymbol{\alpha} = \boldsymbol{\rho} + \boldsymbol{\psi} \end{cases} & (9c) \\
 & \begin{cases} [\boldsymbol{\rho}, \boldsymbol{\psi}] \sim \text{Multi_normal}(\boldsymbol{\beta}, \Omega) \end{cases} & (9d)
 \end{aligned}$$

The mean isotopes ($\mu^{18}O$ and μ^2H) and EC (ε) of stream water are constrained by a mixing model (Eqs. 9a-b), which estimates the isotope and EC mean values of stream water by multiplying the contribution of each runoff component (f_i) with the corresponding mean isotope and EC values of each runoff component (Eq. 9a). In this equation, N is the number of runoff components. The contribution vector (\mathbf{f}) is represented by a Dirichlet distribution with an index vector $\boldsymbol{\alpha}$ (Eq. 9b), in which the sum of contributions of all runoff components ($\sum f_i$) equals one. The index vector $\boldsymbol{\alpha}$ is estimated by two variable vectors $\boldsymbol{\rho}$ and $\boldsymbol{\psi}$ (Eq. 9c), considering the temporal and spatial variability in the CRC (Cable et al. 2011). $\boldsymbol{\rho}$ and $\boldsymbol{\psi}$ are assumed as bivariate



normal distribution with means and precision matrix β and Ω (Eq.9d). β is a parameter vector estimated by likelihood observations (Table 3).

The value ranges for the parameters need to be estimated in Eqs. 6-9 are summarized in Table 3. The posteriors of parameters describing the spatial variability of water tracers in Eqs. 7 and 8b are first estimated by the mean water tracer signatures of runoff components measured at different spatial locations. Parameters describing the overall variability of water tracer signatures in Eqs. 6 and 8a are then constrained by the likelihood observations of water tracer signatures from all water samples at different times and locations. The posterior distribution of CRC (f) are estimated by Eq. 9, based on the posterior water tracer signatures of runoff components and the measured water tracer signatures from stream water samples. The posteriors of parameters and contributions are estimated by the *R* software package *Rstan*. We run four parallel Markov Chain Monte Carlo (MCMC) chains with 2000 iterations for each chain. The first 1000 iterations are discarded for warm-up, generating a total of 4*1000 samples for the calculation of the posterior distributions. Uncertainties are presented as the 5-95 percentile ranges from the iterative runs. The parameter values are assumed to follow uniform prior distributions within the value ranges to run the MCMC procedure.

3.3 Effects of the uncertainty in the meltwater sampling

Due to limited accessibility, meltwater samples are typically difficult to collect in high-elevation glacierized areas. Often, only small sample sizes are available to represent the tracer signatures of meltwater generated from the entire glacierized area. Hence, the representativeness of meltwater samples can have significant effects on the hydrograph separation.

To evaluate this effect for the TEMMA and Bayesian mixing approaches, we define three virtual sampling scenarios. Scenario I: The meltwater sample groups have different sample sizes, but the same mean value and Sd of the investigated tracer; Scenario II: The meltwater sample groups have different mean values of the investigated tracer, but the same sample size and Sd of the investigated tracer; Scenario III: The meltwater sample groups have different Sd of the investigated tracer, but keeping the same sample size and mean value of the investigated tracer. We only investigated the effects of the meltwater sampling uncertainty on the mixing approaches in the glacier melt season, since meltwater is particularly difficult to collect and is the dominant runoff component in this season. For the water samples of other runoff components and stream water, we used all the available measurements in the glacier melt season for the three virtual scenarios, keeping the same sample characteristics.

3.4 Effects of water isotope fractionation on hydrograph separation



To consider the changes on the isotope signatures of runoff components caused by the fractionation effect during the mixing process, we set up two modified Bayesian approaches, i.e. Bayesian_3_Cor_F and Bayesian_4_Cor_F (Table 2). The effects of water isotope fractionation on the hydrograph separation are investigated in virtual experiments using the modified approaches. We modify the mean values in Eq. 9a using fractionation factors $\xi^{18}\text{O}$ and $\xi^2\text{H}$ (Eq. 10). The priors for $\xi^{18}\text{O}$ and $\xi^2\text{H}$ are assumed as bivariate normal distributions in Eq.11.

$$\begin{bmatrix} \mu^{18}\text{O} \\ \mu^2\text{H} \end{bmatrix}_{\text{stream water}} = \sum_{i=1}^N f_i \cdot \begin{bmatrix} \mu^{18}\text{O} + \xi^{18}\text{O} \\ \mu^2\text{H} + \xi^2\text{H} \end{bmatrix}_{\text{runoff component } i} \quad (10)$$

$$\begin{bmatrix} \xi^{18}\text{O} \\ \xi^2\text{H} \end{bmatrix} \sim \text{Multi_normal} \left(\begin{bmatrix} \eta^{18}\text{O} \\ \eta^2\text{H} \end{bmatrix}, \boldsymbol{\Omega} \right) \quad (11)$$

where, $\eta^{18}\text{O}$ and $\eta^2\text{H}$ are the mean values of the changes in isotopes caused by the fractionation effect, which are parameters need to be estimated. $\boldsymbol{\Omega}$ is the inverse of the covariance matrix defined in Eq. 6b. The parameters in Eqs. 6-11 are then re-estimated by the measurements of water tracer signatures using the MCMC procedure.

4. Results

4.1 Seasonality of water tracer signatures

Tracer measurements from all the water samples are summarized in Table 1 and Fig. 2. The mean values indicate that precipitation is most depleted in heavy water isotopes (^{18}O and ^2H) in the cold season among the water sources. In the melt seasons, snow and glacier meltwater show the most depleted heavy isotopes. The EC values are highest in groundwater in all seasons, followed by stream water and precipitation. Snowmelt and glacier melt tend to have the lowest EC values, due to low interaction with mineral surface.

CV values in Table 1 show that the $\delta^{18}\text{O}$ and $\delta^2\text{H}$ of precipitation generally shows the largest variability in all seasons, followed by the isotopes of snowmelt. Groundwater and stream water show the smallest CV values for $\delta^{18}\text{O}$ in all three seasons. The stream water presents the lowest CV value for EC in all seasons, followed by the groundwater. The snowmelt EC shows high CV values in the snowmelt and glacier melt seasons, which may be attributed to variable dust conditions at the sampling locations (from downstream gauge station to upper glacier accumulation zone). The highest CV value of EC was observed for glacier melt, since the glacier melt water samples were collected at locations with different sediments conditions in the ice (from extremely clean to heavily dusty).



For each water source except groundwater, the water tracer signatures show a significant seasonal (Table 1). In particular, the $\delta^{18}\text{O}$ and $\delta^2\text{H}$ of precipitation are most depleted in the cold season and reach the highest values in the glacier melt season, partly caused by the seasonality in temperature. Stream water shows higher values of $\delta^{18}\text{O}$ and EC in the cold season when groundwater dominates the streamflow, and has lower values in the melt seasons when meltwater has a dominant contribution. Snowmelt has a lower EC value in the glacier melt season than in the cold and snowmelt seasons. This can be explained by the fact that the snowmelt samples in glacier melt season were collected from fresh snow in the accumulation area. The water tracer signature of groundwater is relatively stable across the seasons.

Figure 2 shows that the slope of the local meteoric water line (LMWL) is lower than that of the global meteoric water line (GMWL). The $\delta^{18}\text{O}$ of precipitation and snowmelt range from -22.82‰ to 1.51‰ and from -17.31‰ to -6.95‰, respectively. The isotopic composition of glacier meltwater is more depleted than those of groundwater and stream water. Stream water shows a similar isotopic composition to groundwater. Three samples from the stream water are far below the LMWL, which is assumed to be caused by the evaporation effect.

Figure 3 shows the $\delta^{18}\text{O}$ -EC mixing space of runoff components in the three seasons. The uncertainty bars of the tracer values represent the temporal and spatial variability. In the cold season, the $\delta^{18}\text{O}$ and EC values of stream water are very close to those of groundwater (Fig. 3a), whereas the snowmelt and precipitation tracer signatures are different. These results indicate the dominance of groundwater on streamflow during the cold season. In the snowmelt and glacier melt seasons (Figs. 3b-c), the stream water samples are located clearly within the triangle formed by the samples of runoff components. The water tracer signatures of glacier meltwater and snowmelt water are similar. The precipitation samples are farther away from the stream water samples compared to the meltwater and groundwater samples. The stream water samples are located nearly in the middle between the meltwater and groundwater samples. This indicates that the contribution of rainfall to total runoff is smallest and the contributions of meltwater and groundwater are similar, in the melt seasons. We assume the tracer signatures of rainfall are represented by the measurements of precipitation samples three seasons.

4.2 Contributions of runoff components estimated by the mixing approaches

Table 4 and Fig. 4 compare the CRC estimated by multiple mixing approaches. In the cold season (Fig. 4a), the TEMMA_3 estimated the mean contributions of groundwater and snowmelt as 83% and 17%, respectively. The mean contribution of rainfall is zero. The mean contributions of groundwater, snowmelt and rainfall were estimated as 86% (87%), 13% (12%) and 1% (1%) by the Bayesian_3 (Bayesian_3_Cor) approach. As shown in Fig. 3a, the water



363 tracer signature of stream water in this season is close to that of groundwater, while obviously
 364 different from that of rainfall. Meanwhile, the stream water samples are outside of the triangle
 365 formed by the runoff components, leading to the zero contribution of the rainfall estimated by
 366 the TEMMA_3. The ranges for the CRC indicate the uncertainty in the estimates associated
 367 with the corresponding mixing approaches (Table 4). The TEMMA_3 produced the highest
 368 uncertainty for the CRC, followed by the Bayesian_3. The Bayesian_3_Cor slightly reduced
 369 the uncertainty compared to the Bayesian_3, benefiting from the consideration of the
 370 correlation between $\delta^{18}\text{O}$ and $\delta^2\text{H}$.

371 In the snowmelt season (Fig. 4b and Table 4), the TEMMA_3 estimated the mean
 372 contributions of groundwater, rainfall and snowmelt as 44%, 36% and 20%, respectively. The
 373 Bayesian_3 estimated similar mean CRC to the TEMMA_3, whereas the Bayesian_3_Cor
 374 delivered a lower contribution of snowmelt (32%). When treating the glacier melt and snowmelt
 375 as one end-member (i.e. meltwater) in the glacier melt season (Fig. 4c), the TEMMA_3
 376 estimated the mean contributions of groundwater, meltwater and rainfall of 45%, 46% and 9%,
 377 respectively. The Bayesian_3 and Bayesian_3_Cor estimated a lower contribution of
 378 groundwater (43-44%) and a higher contribution of rainfall (11%) compared to the TEMMA_3.
 379 In general, the TEMMA_3 estimated the largest uncertainty for the contributions in all the three
 380 seasons, followed by the Bayesian_3. The Bayesian_3_Cor slightly reduced the uncertainty
 381 ranges compared to the Bayesian_3 (Table 4).

382 When treating glacier melt and snowmelt as two separate end-members in the glacier
 383 melt seasons (Fig. 4d), the TEMMA_4 failed to separate the hydrograph in the glacier melt
 384 season, given the large uncertainty range for the contributions of snowmelt and rainfall (0-
 385 100%). The tracer signatures of snow and glacier meltwater are rather close to each other, that
 386 violates the second assumption of the TEMMA (see Sec. 3.1). In contrast, the Bayesian_4_Cor
 387 and Bayesian_4 estimated the shares of glacier melt and snowmelt as 25-24% and 21-25%,
 388 respectively. Considering the significant snow cover area in September in the study basin (He
 389 et al. 2018; He et al. 2019), the contribution of snowmelt in the glacier melt season should be
 390 much higher than zero. Again, the Bayesian_4_Cor produced smaller uncertainty ranges for the
 391 contributions of groundwater and meltwater compared to the Bayesian_4 and TEMMA_4
 392 (Table 4).

393 The posterior distributions of water tracer signatures estimated by the Bayesian_4_Cor
 394 in the glacier melt season are compared with the measured distributions of water tracers in Fig.
 395 5. The Bayesian_4_Cor generally produced similar distributions of water isotopes to the
 396 measured distributions, in terms of the similar mean values. The estimated posterior Sd values



of the water isotopes are smaller than those of the measured water isotopes. This can be explained by the incorporation of prior distributions by the Bayesian_4_Cor, thus reducing the variability of water isotopes. The posterior Sd values for the EC of water sources are also smaller than the measured Sd values. However, the posterior distributions of EC show some deviations from the distributions of measured EC, partly due to the very small sample sizes (see Table 1). The comparison between the posterior distributions of water tracers estimated by the Bayesian_3_Cor and the measured distributions in the other seasons generally shows a similar behavior (not shown for brevity).

The Bayesian_4 estimated similar posterior distributions of water tracer signatures to the Bayesian_4_Cor (except the glacier melt isotopes, Fig. 6), with similar mean tracer values and Sd . It is noted that the Bayesian_4_Cor estimated smaller Sd values for most water sources than the Bayesian_4 (e.g., Figs. 6f-g and 6i-j). Benefiting from the prior information and the consideration of the correlation between $\delta^{18}\text{O}$ and $\delta^2\text{H}$, the Bayesian_4_Cor tended to produce the smallest variability in the posterior water tracers among the mixing approaches (Figs. 5-6), thus resulting in the smallest uncertainty for CRC (Fig. 4d). Figure 7 compares the correlation between $\delta^{18}\text{O}$ and $\delta^2\text{H}$ in the measured tracers and the posterior estimates by the Bayesian approaches. The Bayesian_4_Cor reproduced the correlation between $\delta^{18}\text{O}$ and $\delta^2\text{H}$ well in comparison to the measured data, whereas the Bayesian_4 failed to capture the correlation.

4.3 Uncertainty for hydrograph separation caused by sampling uncertainty of meltwater

Figure 8 shows the sensitivity of the Bayesian_3_Cor and TEMMA_3 approaches to the sampled $\delta^{18}\text{O}$ of meltwater in the glacier melt season. The mean CRC quantified by the two mixing approaches show minor sensitivity to the sample size (scenario I). However, the uncertainty ranges for the contributions tend to decrease with increasing sample size, especially for the TEMMA_3. When assuming only two meltwater samples, the TEMMA_3 resulted in very large uncertainty ranges (0-100%), due to the very wide confidence interval for the Sd at a sample size of two. The mean contributions of groundwater and meltwater estimated by the two mixing approaches decrease with increasing mean $\delta^{18}\text{O}$ of the adopted meltwater sample (scenario II), while the estimated contribution of rainfall increases with the increasing mean $\delta^{18}\text{O}$. The variations in the mean CRC quantified by the TEMMA_3 are larger than those estimated by the Bayesian_3_Cor. In the TEMMA_3, both the mean contributions of groundwater and meltwater declined by 9% with the assumed increase of the mean $\delta^{18}\text{O}$, and the contribution of rainfall increased by 17%. In the Bayesian_3_Cor, the reduction for the contributions of groundwater and snowmelt are 4% and 7%, respectively, and the increase for the contribution of rainfall is 11%. In scenario III, the uncertainty ranges for the CRC



(especially for rainfall, Fig. 8l) increase with increasing Sd of the sampled $\delta^{18}\text{O}$. Again, the increases in the uncertainty ranges estimated by the TEMMA_3 tend to be larger than those estimated by the Bayesian_3_Cor. The sensitivity of the mixing approaches to the sampled EC values of the meltwater are similar to the sensitivity to the sampled $\delta^{18}\text{O}$ (not shown).

4.4 Effect of isotope fractionation on the hydrograph separation

The changes of $\delta^{18}\text{O}$ caused by the fractionation effect during the mixing process are estimated in Figs. 9a-c. The fractionation has the smallest effect on the $\delta^{18}\text{O}$ of groundwater, while the largest effect on the $\delta^{18}\text{O}$ of rainfall. Averagely, the $\delta^{18}\text{O}$ of rainfall was increased by around 2.8‰ through the fractionation. The CRC estimated by the Bayesian_3_Cor_F and Bayesian_4_Cor_F are compared with those estimated by the Bayesian_3_Cor and Bayesian_4_Cor in Figs. 9d-f, respectively. The mean contribution of groundwater estimated by the Bayesian_3_Cor_F in the cold season is 9% lower than that estimated by the Bayesian_3_Cor (Fig. 9d), while the mean contributions of snowmelt and rainfall are 3% and 5% higher, respectively. The reduction of groundwater contribution is the compensation for the increased contributions of snowmelt and rainfall caused by the fractionation effect. In the snowmelt season, the mean contributions of groundwater and rainfall are 1% and 7% lower (Fig. 9e), while the mean contribution of snowmelt estimated by the Bayesian_3_Cor_F is 8% higher. In the glacier melt season, the mean contributions of groundwater and meltwater estimated by the Bayesian_4_Cor_F are higher than those estimated by the Bayesian_4_Cor (Fig. 9f) and are compensated by the 6% lower contribution of rainfall.

The fractionation effect also produced visible changes on the posterior distributions of $\delta^{18}\text{O}$ and $\delta^2\text{H}$ of runoff components (Fig. 10 shows the example in the glacier melt season). The mean isotopic compositions of runoff components are increased by the fractionation effect. The Sd values of the posterior isotopes estimated by the Bayesian_4_Cor_F tend to be higher than those estimated by the Bayesian_4_Cor, due to the increased parameter space in the prior assumptions (Eq. 11), thus leading to the larger uncertainty ranges for the contributions of glacier melt and snowmelt (Fig. 9f). As expected, the estimates for the posterior distributions of isotopic compositions of stream water are less sensitive to the fractionation effect of runoff components (Figs. 10e and 10j). The fractionation also has minor effects on the estimates for the posterior distributions of EC values (Figs. 10k-o).

5. Discussion

5.1 Uncertainty for the contributions of runoff components

The TEMMA estimated larger uncertainties for the CRC in comparison to the Bayesian approaches. The reasons for this are two-fold. First, the TEMMA estimated the uncertainty



465 ranges for the CRC using the standard deviations (S_d) of the measured water tracer signatures.
466 S_d is likely overestimated, due to small sample size and thus insufficiently represents the
467 variability of the tracers of the corresponding water sources. Due to the limited accessibility of
468 the sampled sites caused by snow cover, the water samples of meltwater and groundwater are
469 often collected occasionally, thus leading to sharp changes in the measured water tracer
470 signatures. Second, the TEMMA assumes that the uncertainty associated with each water source
471 is independent from the uncertainty of other water sources (Eq.5), which increases the
472 uncertainty ranges for CRC.

473 In contrast, the Bayesian approaches estimated smaller variability of water tracer
474 signatures in the posterior distributions compared to the measured water tracer signatures, by
475 updating the prior probability distributions. The posterior distributions were sampled
476 continuously from the assumed value ranges, thus reducing the sharp changes and yielding
477 lower variability for the tracer signatures. Moreover, the uncertainty ranges for CRC were
478 quantified using Eqs. 6-10, instead of calculating independently as in the TEMMA.
479 Additionally, the assumed prior distributions for the water tracers and the CRC take into
480 account the correlation between the water tracers and the dependence between the runoff
481 components in the Bayesian approaches, thus resulting in smaller uncertainty ranges (Soulsby
482 et al., 2003). For example, the Bayesian approaches considering the correlation between $\delta^{18}\text{O}$
483 and $\delta^2\text{H}$ generally estimated smaller uncertainty ranges for CRC compared to those without
484 considering this correlation.

485 The Gaussian error propagation technique is only capable of considering the uncertainty
486 for the CRC resulting from the variation in the water tracer signatures (Uhlenbrook and Hoeg,
487 2003). The uncertainty for CRC originated from the sampling uncertainty of meltwater was
488 then investigated in separate virtual sampling experiments. The TEMMA produces large
489 uncertainty ranges in the glacier melt season, when the meltwater sample size is rather small.
490 The mean CRC quantified by the TEMMA relies more heavily on the mean tracer values of the
491 sampled meltwater, as the mean tracer values are directly used in Eqs. 1-4, in comparison to the
492 mean CRC estimated by the Bayesian approach.

493 The TEMMA assumes that the water tracer signature of each runoff component is
494 constant during the mixing process, thus is unable to estimate the uncertainty for CRC caused
495 by the isotope fractionation effect. The virtual fractionation experiments using the modified
496 Bayesian approaches show that the isotope fractionation could increase the contribution of
497 snowmelt by 8%, and reduce the contribution of rainfall by 7% in the snowmelt season. We
498 assume the mean CRC estimated by the Bayesian approaches considering the isotope



fractionation are more plausible, though the larger uncertainty ranges. Along the flow path from the source areas to river, the isotopic compositions of meltwater and rainfall are likely increased by the evaporation fractionation effect, especially in the warm seasons. The increased isotopic compositions of meltwater and rainfall during the routing process need to be considered in the mixing approaches for hydrograph separation.

In general, the uncertainty for the CRC is visibly caused by the spatio-temporal variability in the water tracer signatures, the water sampling uncertainty and the isotope fractionation during the mixing process. The uncertainty caused by the water sampling of meltwater tends to be smaller than the uncertainty caused by the variations of the water tracer signatures in both the TEMMA and Bayesian mixing approaches. This is consistent to the findings that the S_d values in the tracer measurements of water samples are the main uncertainty sources for the CRC (Schmieder et al., 2016; Schmieder et al., 2018). The Bayesian approach tends to be superior in narrowing the variability of posterior water tracer signatures benefiting from the prior assumptions and the consideration of the dependence between water tracer signatures and runoff components compared to the TEMMA.

5.2 Limitations

The representativeness of the water samples is one of the limitations of this study. The groundwater was only sampled from a single spring located at the elevation of 2400 m a.s.l., which is rather close to the average altitude of the entire river network in the study basin (2530 m a.s.l.). We thus assume that the measured isotopic composition of the spring water represents the mean isotopic composition of groundwater feeding the river in the basin (similarly to He et al., 2019). Collecting samples from a few spring points to represent the groundwater end-member has been proposed before (such as Ohlanders et al., 2013 and Mark and McKenzie, 2007), as the accessibility and availability of more potential springs are hampered. Again, for the snow and glacier meltwater samples, we assume that meltwater occurring at similar elevations have similar water tracer signatures (He et al., 2019). The sampled elevation ranges from 1580 m to 4050 m a.s.l., matching with the elevation range where meltwater mainly occurs in the basin (from 1580 m to 3950 m a.s.l.). The sampled sites thus bear the potential to provide the water tracer signatures for the major share of the meltwater generated in the basin. We divided the entire sampling period (years of 2012 to 2017) into three seasons, i.e. cold season, snowmelt season and glacier melt season, due to the low availability of water samples in each year. By concentrating water samples in the three seasons, we increased the sample sizes of each runoff component for each season, thus increasing the ability of water samples to represent the spatio-temporal variability of seasonal tracer signatures.



533 The assumptions of the mixing approaches lead to another limitation of this study. The
 534 TEMMA assumes the tracer signatures of water sources are constant during the mixing process,
 535 which is a common assumption for TEMMA. It thus fails to consider the uncertainty originating
 536 from the changes of water tracers. In the Bayesian approach, we assumed normal prior
 537 distributions for the water tracers of water sources and Dirichlet prior distribution for the CRC
 538 by literature knowledge (Cable et al., 2011). To refine the description of the temporal and spatial
 539 variability of the CRC in the Dirichlet distribution, more hydrological data relating to the runoff
 540 processes in the basin are required. We acknowledge that the estimated CRC could be strongly
 541 affected by the assumptions of prior distributions. However, testing the effects of the prior
 542 assumptions goes beyond the scope of this study. We assume that collecting more water
 543 samples from various locations and at different time for each water source could improve the
 544 estimation for the tracer signature distributions.

545 6. Conclusions

546 This study compared the Bayesian end-member mixing approach with a traditional end-
 547 member mixing approach (TEMMMA) for hydrograph separation in a glacierized basin. The
 548 contributions of runoff components (CRC) to the total runoff were estimated for three seasons,
 549 i.e. cold season, snowmelt and glacier melt seasons. Uncertainty for these contributions caused
 550 by the variability of water tracer signatures, water sampling uncertainty and isotope
 551 fractionation were evaluated as follows.

552 (1) The Bayesian approach generally estimates smaller uncertainty ranges for the CRC,
 553 in comparison to the TEMMA. Benefiting from the prior assumptions on water tracer signatures
 554 and CRC, as well as from the incorporation of the correlation between tracer signatures in the
 555 prior distributions, the Bayesian approach reduced the uncertainty. The Bayesian approach
 556 jointly quantified the uncertainty ranges for the CRC. In contrast, the TEMMA estimated the
 557 uncertainty for the contribution of each runoff component independently, thus leading to higher
 558 uncertainty ranges.

559 (2) The estimates for CRC in the TEMMA tend to be more sensitive to the sampling
 560 uncertainty of meltwater, compared to those in the Bayesian approach. For small sample sizes
 561 (e.g., two), the TEMMA estimated very large uncertainty ranges. The mean CRC quantified by
 562 the TEMMA are also more sensitive to the mean value of the tracer signature of the meltwater
 563 samples than those estimated by the Bayesian approach are.

564 (3) Ignoring the isotope fractionation during the mixing process likely overestimates the
 565 contribution of rainfall and underestimates the contribution of meltwater in the melt seasons.



566 The currently used TEMMA is unable to quantify the uncertainty for CRC caused by the isotope
567 fractionation during the mixing process, due to the underlying assumptions.



568 Code availability: The R code for the Bayesian end-member mixing approach can be found at
569 [https://www.dropbox.com/s/kf2xy3s4vt718s9/Bayesian%20mixing%20approach_four%20co](https://www.dropbox.com/s/kf2xy3s4vt718s9/Bayesian%20mixing%20approach_four%20components.stan?dl=0)
570 [mponents.stan?dl=0](https://www.dropbox.com/s/kf2xy3s4vt718s9/Bayesian%20mixing%20approach_four%20components.stan?dl=0)

571

572 Author contributions.

573 Conceptualization: Zhihua He, Katy Unger-Shayesteh, and Sergiy Vorogushyn; Data collection:
574 Zhihua He, Katy Unger-Shayesteh, Stephan M. Weise, Olga Kalashnikova, and Abror Gafurov;
575 Methodology: Zhihua He, Katy Unger-Shayesteh, and Sergiy Vorogushyn; Writing original
576 draft: Zhihua He, Sergiy Vorogushyn, and Doris Duethmann; Writing review and editing, All

577

578 Competing interests.

579 The authors declare no conflict of interest.

580

581

582 **Acknowledgement**

583 Our work has been funded by the German Federal Ministry for Science and Education (project
584 GlaSCA-V, grant number 88 501) and Volkswagen Foundation (project GlaSCA, grant number
585 01DK15002A and B), respectively.



586 **Reference**

- 587 Aizen, V., Aizen, E., Glazirin, G., and Loaiciga, H. A.: Simulation of daily runoff in Central
 588 Asian alpine watersheds, *Journal of Hydrology*, 238, 15-34,
 589 [https://doi.org/10.1016/S0022-1694\(00\)00319-X](https://doi.org/10.1016/S0022-1694(00)00319-X), 2000.
- 590 Aizen, V. B., Aizen, E. M., and Melack, J. M.: Precipitation, melt and runoff in the northern
 591 Tien Shan, *Journal of Hydrology*, 186, 229-251, [https://doi.org/10.1016/S0022-](https://doi.org/10.1016/S0022-1694(96)03022-3)
 592 [1694\(96\)03022-3](https://doi.org/10.1016/S0022-1694(96)03022-3), 1996.
- 593 Aizen, V. B., Kuzmichenok, V. A., Surazakov, A. B., and Aizen, E. M.: Glacier changes in the
 594 Tien Shan as determined from topographic and remotely sensed data, *Global and*
 595 *Planetary Change*, 56, 328-340, <https://doi.org/10.1016/j.gloplacha.2006.07.016>, 2007.
- 596 Barnett, T. P., Adam, J. C., and Lettenmaier, D. P.: Potential impacts of a warming climate on
 597 water availability in snow-dominated regions, *Nature*, 438, 303–309,
 598 [doi:10.1038/nature04141](https://doi.org/10.1038/nature04141), 2005.
- 599 Beria, H., Larsen, J. R., Michelon, A., Ceperley, N. C., and Schaepli, B.: HydroMix v1.0: a new
 600 Bayesian mixing framework for attributing uncertain hydrological sources,
 601 *Geoscientific Model Development Discussion*, <https://doi.org/10.5194/gmd-2019-69>, in
 602 review, 2019.
- 603 Brown, L. E., Hannah, D. M., Milner, A. M., Soulsby, C., Hodson, A. J., and Brewer, M. J.:
 604 Water source dynamics in a glacierized alpine river basin (Taillon-Gabietous, French
 605 Pyrenees), *Water Resources Research*, 42, W08404, [doi:10.1029/2005WR004268](https://doi.org/10.1029/2005WR004268),
 606 2006.
- 607 Cable, J., Ogle, K., and Williams, D.: Contribution of glacier meltwater to streamflow in the
 608 Wind River Range, Wyoming, inferred via a Bayesian mixing model applied to isotopic
 609 measurements, *Hydrological Processes*, 25, 2228-2236, [doi:10.1002/hyp.7982](https://doi.org/10.1002/hyp.7982), 2011.
- 610 Chiogna, G., Santoni, E., Camin, F., Tonon, A., Majone, B., Trenti, A., and Bellin, A.: Stable
 611 isotope characterization of the Vermigliana catchment, *Journal of Hydrology*, 509, 295-
 612 305, <https://doi.org/10.1016/j.jhydrol.2013.11.052>, 2014.
- 613 Dahlke, H. E., Lyon, S. W., Jansson, P., Karlin, T., and Rosqvist, G.: Isotopic investigation of
 614 runoff generation in a glacierized catchment in northern Sweden, *Hydrological*
 615 *Processes*, 28, 1383-1398, [doi:10.1002/hyp.9668](https://doi.org/10.1002/hyp.9668), 2014.
- 616 Engel, M., Penna, D., Bertoldi, G., Dell'Agnese, A., Soulsby, C., and Comiti, F.: Identifying
 617 run-off contributions during melt-induced run-off events in a glacierized alpine
 618 catchment, *Hydrological Processes*, 30, 343-364, [doi:10.1002/hyp.10577](https://doi.org/10.1002/hyp.10577), 2016.



- 619 Genereux, D.: Quantifying uncertainty in tracer-based hydrograph separations, *Water*
 620 *Resources Research*, 34, 915-919, <https://doi.org/10.1029/98WR00010>, 1998.
- 621 He, Z. H., Parajka, J., Tian, F. Q., and Blöschl, G.: Estimating degree-day factors from MODIS
 622 for snowmelt runoff modeling, *Hydrology and Earth System Sciences*, 18, 4773–4789,
 623 <https://doi.org/10.5194/hess-18-4773-2014>, 2014.
- 624 He, Z. H., Tian, F. Q., Gupta, H. V., Hu, H. C., and Hu, H. P.: Diagnostic calibration of a
 625 hydrological model in a mountain area by hydrograph partitioning, *Hydrology and Earth*
 626 *System Sciences*, 19, 1807–1826, <https://doi.org/10.5194/hess-19-1807-2015>, 2015.
- 627 He, Z., Unger-Shayesteh, K., Vorogushyn, S., Weise, S. M., Kalashnikova, O., Gafurov, A.,
 628 Duethmann, D., Barandun, M., and Merz, B.: Constraining hydrological model
 629 parameters using water isotopic compositions in a glacierized basin, Central Asia,
 630 *Journal of Hydrology*, 571, 332-348, <https://doi.org/10.1016/j.jhydrol.2019.01.048>,
 631 2019.
- 632 He, Z., Vorogushyn, S., Unger-Shayesteh, K., Gafurov, A., Kalashnikova, O., Omorova, E.,
 633 and Merz, B.: The Value of Hydrograph Partitioning Curves for Calibrating
 634 Hydrological Models in Glacierized Basins, *Water Resources Research*, 54, 2336-2361,
 635 doi.org/10.1002/2017WR021966, 2018.
- 636 Joerin, C., Beven, K. J., Iorgulescu, I., and Musy, A.: Uncertainty in hydrograph separations
 637 based on geochemical mixing models, *Journal of Hydrology*, 255, 90-106,
 638 [https://doi.org/10.1016/S0022-1694\(01\)00509-1](https://doi.org/10.1016/S0022-1694(01)00509-1), 2002.
- 639 Klaus, J., and McDonnell, J. J.: Hydrograph separation using stable isotopes: Review and
 640 evaluation, *Journal of Hydrology*, 505, 47-64, [https://doi.org/10.1016/j.jhydrol.2013.09.](https://doi.org/10.1016/j.jhydrol.2013.09.006)
 641 006, 2013.
- 642 Kong, Y. L., and Pang, Z. H.: Evaluating the sensitivity of glacier rivers to climate change
 643 based on hydrograph separation of discharge, *Journal of Hydrology*, 434, 121-129,
 644 <https://doi.org/10.1016/j.jhydrol.2012.02.029>, 2012.
- 645 La Frenierre, J., and Mark, B. G.: A review of methods for estimating the contribution of glacial
 646 meltwater to total watershed discharge, *Progress in Physical Geography*, 38, 173-200,
 647 [doi:10.1177/0309133313516161](https://doi.org/10.1177/0309133313516161), 2014.
- 648 Li, Z. X., Feng, Q., Liu, W., Wang, T. T., Cheng, A. F., Gao, Y., Guo, X. Y., Pan, Y. H., Li, J.
 649 G., Guo, R., and Jia, B.: Study on the contribution of cryosphere to runoff in the cold
 650 alpine basin: A case study of Hulugou River Basin in the Qilian Mountains, *Global and*
 651 *Planetary Change*, 122, 345-361, <https://doi.org/10.1016/j.gloplacha.2014.10.001>, 2014.



- 652 Mark, B. G., and McKenzie, J. M.: Tracing increasing tropical Andean glacier melt with stable
 653 isotopes in water, *Environmental Science & Technology*, 41, 6955-6960,
 654 <https://doi.org/10.1021/es071099d>, 2007.
- 655 Maurya, A. S., Shah, M., Deshpande, R. D., Bhardwaj, R. M., Prasad, A., and Gupta, S. K.:
 656 Hydrograph separation and precipitation source identification using stable water
 657 isotopes and conductivity: River Ganga at Himalayan foothills, *Hydrological Processes*,
 658 25, 1521-1530, doi:10.1002/hyp.7912, 2011.
- 659 Moore, J. W., and Semmens, B. X.: Incorporating uncertainty and prior information into stable
 660 isotope mixing models, *Ecology Letters*, 11, 470-480, doi:10.1111/j.1461-
 661 0248.2008.01163.x, 2008.
- 662 Ohlanders, N., Rodriguez, M., and McPhee, J.: Stable water isotope variation in a Central
 663 Andean watershed dominated by glacier and snowmelt, *Hydrology and Earth System*
 664 *Sciences*, 17, 1035-1050, doi:10.5194/hess-17-1035-2013, 2013.
- 665 Parnell, A. C., Inger, R., Bearhop, S., and Jackson, A. L.: Source Partitioning Using Stable
 666 Isotopes: Coping with Too Much Variation, *PLoS ONE* 5(3): e9672.
 667 doi:10.1371/journal.pone.0009672, doi:10.1371/journal.pone.0009672, 2010.
- 668 Penna, D., Engel, M., Bertoldi, G., and Comiti, F.: Towards a tracer-based conceptualization of
 669 meltwater dynamics and streamflow response in a glacierized catchment, *Hydrology*
 670 *and Earth System Sciences*, 21, 23-41, doi:10.5194/hess-21-23-2017, 2017.
- 671 Penna, D., Engel, M., Mao, L., Dell'Agnese, A., Bertoldi, G., and Comiti, F.: Tracer-based
 672 analysis of spatial and temporal variations of water sources in a glacierized catchment,
 673 *Hydrology and Earth System Sciences*, 18, 5271-5288, doi:10.5194/hess-18-5271-2014,
 674 2014.
- 675 Penna, D., van Meerveld, H. J., Zuecco, G., Fontana, G. D., and Borga, M.: Hydrological
 676 response of an Alpine catchment to rainfall and snowmelt events, *Journal of Hydrology*,
 677 537, 382-397, <https://doi.org/10.1016/j.jhydrol.2016.03.040>, 2016.
- 678 Pohl, E., Gloaguen, R., Andermann, C., and Knoche, M.: Glacier melt buffers river runoff in
 679 the Pamir Mountains, *Water Resources Research*, 53, 2467-2489,
 680 doi:10.1002/2016WR019431, 2017.
- 681 Pu, T., He, Y. Q., Zhu, G. F., Zhang, N. N., Du, J. K., and Wang, C. F.: Characteristics of water
 682 stable isotopes and hydrograph separation in Baishui catchment during the wet season
 683 in Mt. Yulong region, south western China, *Hydrological Processes*, 27, 3641-3648, doi:
 684 10.1002/hyp.9479, 2013.



- 685 Pu, T., Qin, D. H., Kang, S. C., Niu, H. W., He, Y. Q., and Wang, S. J.: Water isotopes and
 686 hydrograph separation in different glacial catchments in the southeast margin of the
 687 Tibetan Plateau, *Hydrological Processes*, 31, 3810-3826, doi:10.1002/hyp.11293, 2017.
- 688 Rahman, K., Besacrier-Monbertrand, A. L., Castella, E., Lods-Crozet, B., Ilg, C., and Beguin,
 689 O.: Quantification of the daily dynamics of streamflow components in a small alpine
 690 watershed in Switzerland using end member mixing analysis, *Environmental Earth*
 691 *Sciences*, 74, 4927-4937, <https://doi.org/10.1007/s12665-015-4505-5>, 2015.
- 692 Schmieder, J., Garvelmann, J., Marke, T., and Strasser, U.: Spatio-temporal tracer variability
 693 in the glacier melt end-member How does it affect hydrograph separation results,
 694 *Hydrological Processes*, 32, 1828-1843, doi:10.1002/hyp.11628, 2018.
- 695 Schmieder, J., Hanzer, F., Marke, T., Garvelmann, J., Warscher, M., Kunstmann, H., and
 696 Strasser, U.: The importance of snowmelt spatiotemporal variability for isotope-based
 697 hydrograph separation in a high-elevation catchment, *Hydrology and Earth System*
 698 *Sciences*, 20, 5015-5033, doi:10.5194/hess-20-5015-2016, 2016.
- 699 Soulsby, C., Petry, J., Brewer, M. J., Dunn, S. M., Ott, B., and Malcolm, I. A.: Identifying and
 700 assessing uncertainty in hydrological pathways: a novel approach to end member mixing
 701 in a Scottish agricultural catchment, *Journal of Hydrology*, 274, 109-128,
 702 [https://doi.org/10.1016/S0022-1694\(02\)00398-0](https://doi.org/10.1016/S0022-1694(02)00398-0), 2003.
- 703 Sun, C. J., Chen, Y. N., Li, W. H., Li, X. G., and Yang, Y. H.: Isotopic time series partitioning
 704 of streamflow components under regional climate change in the Urumqi River,
 705 northwest China, *Hydrological Sciences Journal-Journal Des Sciences Hydrologiques*,
 706 61, 1443-1459, doi:10.1080/02626667.2015.1031757, 2016a.
- 707 Sun, C. J., Yang, J., Chen, Y. N., Li, X. G., Yang, Y. H., and Zhang, Y. Q.: Comparative study
 708 of streamflow components in two inland rivers in the Tianshan Mountains, Northwest
 709 China, *Environmental Earth Sciences*, 75:727. doi:10.1007/s12665-016-5314-1, 2016b.
- 710 Uhlenbrook, S., and Hoeg, S.: Quantifying uncertainties in tracer-based hydrograph separations:
 711 a case study for two-, three- and five-component hydrograph separations in a
 712 mountainous catchment, *Hydrological Processes*, 17, 431-453, doi:10.1002/hyp.1134
 713 2003.
- 714 Viviroli, D., Durr, H. H., Messerli, B., Meybeck, M., and Weingartner, R.: Mountains of the
 715 world, water towers for humanity: Typology, mapping, and global significance, *Water*
 716 *Resources Research*, 43, W07447, <https://doi.org/10.1029/2006wr005653>, 2007.



717 Ward, E. J., Semmens, B. X., and Schindler, D. E.: Including Source Uncertainty and Prior
718 Information in the Analysis of Stable Isotope Mixing Models, *Environmental Science*
719 & Technology, 44, 4645-4650, doi:10.1021/es100053v, 2010.



720	LIST OF TABLES	
721	Table 1. Water tracer signatures measured from water samples in three seasons	27
722	Table 2. Mixing approaches used for hydrograph separation in different seasons	28
723	Table 3. Parameters used for the prior distributions in the Bayesian approaches.....	29
724	Table 4. Contributions of runoff components estimated by the different mixing approaches	
725	(%).....	30



Table 1. Water tracer signatures measured from water samples in three seasons. CV is the ratio between the standard deviation and mean value.

Season	Water source	Tracer	Sample size	Mean	Range	CV
Cold season (October to February)	Groundwater	^{18}O (‰)	23	-11.37	(-12.12, -10.61)	0.04
		^2H (‰)	23	-73.9	(-77.9, -68.2)	0.03
		EC(μs/cm)	13	126.8	(69.6, 167.2)	0.24
	Precipitation	^{18}O (‰)	37	-15.93	(-22.82, -7.70)	0.21
		^2H (‰)	37	-111.5	(-168.8, -39.1)	0.27
		EC(μs/cm)	23	67.8	(21.3, 99.6)	0.34
	Snowmelt	^{18}O (‰)	36	-12.51	(-17.31, -6.95)	0.19
		^2H (‰)	36	-84.6	(-120.7, -38.7)	0.23
		EC(μs/cm)	15	53.7	(8.8, 151)	0.96
	Stream water	^{18}O (‰)	150	-11.33	(-11.82, -9.05)	0.03
		^2H (‰)	150	-74.2	(-77.5, -68.2)	0.03
		EC(μs/cm)	90	112.2	(80.3, 139.3)	0.13
Snowmelt season (March to June)	Groundwater	^{18}O (‰)	9	-11.34	(-11.94, -11.06)	0.02
		^2H (‰)	9	-73.9	(-77.3, -72.4)	0.02
		EC(μs/cm)	8	133.1	(94, 167.2)	0.21
	Precipitation	^{18}O (‰)	25	-7.89	(-16.81, -0.06)	0.46
		^2H (‰)	25	-49.2	(-120.5, -3.9)	0.52
		EC(μs/cm)	11	58.3	(25.8, 84.3)	0.34
	Snowmelt	^{18}O (‰)	15	-13.87	(-16.74, -10.96)	0.11
		^2H (‰)	15	-95.9	(-119.3, -70.5)	0.13
		EC(μs/cm)	11	67.3	(11.0, 151.0)	0.80
	Stream water	^{18}O (‰)	126	-11.58	(-12.91, -10.04)	0.04
		^2H (‰)	126	-76.1	(-86.4, -67.0)	0.04
		EC(μs/cm)	23	94.9	(80.1, 114.0)	0.09
Glacier melt season (July to September)	Groundwater	^{18}O (‰)	14	-11.4	(-12.12, -10.61)	0.04
		^2H (‰)	14	-73.9	(-77.9, -68.2)	0.04
		EC(μs/cm)	5	116.7	(69.6, 142.6)	0.30
	Precipitation	^{18}O (‰)	28	-6.72	(-13.02, 1.51)	0.56
		^2H (‰)	28	-42.6	(-94.9, 3.0)	0.58
		EC(μs/cm)	9	67.7	(26.7, 102.0)	0.39
	Snowmelt	^{18}O (‰)	15	-12.70	(-17.31, -9.85)	0.15
		^2H (‰)	15	-85.6	(-120.7, -64.0)	0.17
		EC(μs/cm)	4	16.2	(8.8, 24.3)	0.51
	Glacier melt	^{18}O (‰)	23	-13.11	(-14.96, -11.55)	0.10
		^2H (‰)	23	-87.2	(-100.4, -75.5)	0.11
		EC(μs/cm)	10	9.9	(1.5, 33.4)	1.28
	Stream water	^{18}O (‰)	119	-11.75	(-12.97, -5.64)	0.07
		^2H (‰)	119	-77.2	(-86.7, -62.3)	0.05
		EC(μs/cm)	24	64.5	(33.4, 99.3)	0.25



729 Table 2. Mixing approaches used for hydrograph separation in different seasons.

Mixing approach	Description	End-member	Used tracers	Seasons applied to
TEMMA_3	Three-component traditional end-member mixing approach	Groundwater, snowmelt (or meltwater) and rainfall	^{18}O and EC	Cold season, snowmelt season and glacier melt season
TEMMA_4	Four-component traditional end-member mixing approach	Groundwater, snowmelt, glacier melt and rainfall	^{18}O , ^2H and EC	Glacier melt season
Bayesian_3	Three-component Bayesian approach, without considering the correlation between $\delta^{18}\text{O}$ and $\delta^2\text{H}$	Groundwater, snowmelt (or meltwater) and rainfall	^{18}O and EC	Cold season, snowmelt season and glacier melt season
Bayesian_3_Cor	Three-component Bayesian approach, considering the correlation between $\delta^{18}\text{O}$ and $\delta^2\text{H}$	Groundwater, snowmelt (or meltwater) and rainfall	^{18}O , ^2H and EC	Cold season, snowmelt season and glacier melt season
Bayesian_3_Cor_F	Three-component Bayesian approach, considering the correlation between $\delta^{18}\text{O}$ and $\delta^2\text{H}$ and the fractionation of $\delta^{18}\text{O}$ and $\delta^2\text{H}$ during the mixing process	Groundwater, snowmelt and rainfall	^{18}O , ^2H and EC	Cold season and snowmelt season
Bayesian_4	Four-component Bayesian approach, without considering the correlation between ^{18}O and ^2H	Groundwater, snowmelt, glacier melt and rainfall	^{18}O , ^2H and EC	Glacier melt season
Bayesian_4_Cor	Four-component Bayesian approach, considering the correlation between $\delta^{18}\text{O}$ and $\delta^2\text{H}$	Groundwater, snowmelt, glacier melt and rainfall	^{18}O , ^2H and EC	Glacier melt season
Bayesian_4_Cor_F	Four-component Bayesian approach, considering the correlation between $\delta^{18}\text{O}$ and $\delta^2\text{H}$ and the fractionation of $\delta^{18}\text{O}$ and $\delta^2\text{H}$ during the mixing process	Groundwater, snowmelt, glacier melt and rainfall	^{18}O , ^2H and EC	Glacier melt season

730



731 Table 3. Parameters used for the prior distributions in the Bayesian approaches.

Parameter	Description	Applied Bayesian approach	Value range	Equation
$\gamma^{18}\text{O}$	Mean of the prior normal distributions for the mean $\delta^{18}\text{O}$ of runoff components	All Bayesian approaches	(-50,50)	Eq.7a
$\gamma^2\text{H}$	Mean of the prior normal distributions for the mean $\delta^2\text{H}$ of runoff components	All Bayesian approaches, except Bayesian_3	(-200,200)	Eq.7b
$\sigma^{18}\text{O}$	Variance of the prior normal distributions for the mean $\delta^{18}\text{O}$ of runoff components	All Bayesian approaches	(0,50)	Eq.7a
$\sigma^2\text{H}$	Variance of the prior normal distributions for the mean $\delta^2\text{H}$ of runoff components	All Bayesian approaches, except Bayesian_3	(0,200)	Eq.7b
$\lambda^{18}\text{O}$	Variance of the prior normal distributions for the $\delta^{18}\text{O}$ of runoff components and stream water	Bayesian_3 and Bayesian_4	(0,50)	Eq.6c
$\lambda^2\text{H}$	Variance of the prior normal distributions for the $\delta^2\text{H}$ of runoff components and stream water	Bayesian_4	(0,200)	Eq.6d
τ	Variance of the prior normal distributions for the EC of runoff components and stream water	All Bayesian approaches	(0,400)	Eq.8a
θ	Mean of the prior normal distributions for the mean EC of runoff components	All Bayesian approaches	(0,400)	Eq.8b
ω	Variance of the prior normal distributions for the mean EC of runoff components	All Bayesian approaches	(0,400)	Eq.8b
β	Mean of the prior bivariate normal distributions for parameters describing the α value in the Dirichlet distribution of contributions of runoff components	All Bayesian approaches	(0,10)	Eq.9d
$\eta^{18}\text{O}$	Mean of the prior bivariate normal distributions for the fractionations of $\delta^{18}\text{O}$ of runoff components	Bayesian_3_Cor_F and Bayesian_4_Cor_F	(0,5)	Eq.11
$\eta^2\text{H}$	Mean of the prior bivariate normal distributions for the fractionations of $\delta^2\text{H}$ of runoff components	Bayesian_3_Cor_F and Bayesian_4_Cor_F	(0,5)	Eq.11

732



Table 4. Contributions of runoff components (CRC) estimated by the different mixing approaches (%). The ranges show the difference between the 95% and 5% percentiles.

	Mixing approach	Groundwater		Snowmelt		Rainfall		Glacier melt		Meltwater	
		Mean	Range	Mean	Range	Mean	Range	Mean	Range	Mean	Range
Cold season	TEMMA_3	83	47	17	46	0	10	-	-	-	-
	Bayesian_3	86	28	13	28	1	3	-	-	-	-
	Bayesian_3_Cor	87	24	12	24	1	3	-	-	-	-
Snowmlet season	TEMMA_3	44	50	36	33	20	25	-	-	-	-
	Bayesian_3	42	33	36	22	22	20	-	-	-	-
	Bayesian_3_Cor	46	30	32	20	22	19	-	-	-	-
Glacier melt season (three-component)	TEMMA_3	45	48	-	-	9	17	-	-	46	35
	Bayesian_3	43	25	-	-	11	13	-	-	46	18
	Bayesian_3_Cor	44	24	-	-	11	12	-	-	45	17
Glacier melt season (four-component)	TEMMA_4	45	48	0	100	11	100	44	78	-	-
	Bayesian_4	44	30	21	42	10	13	25	41	-	-
	Bayesian_4_Cor	41	23	25	33	10	13	24	33	-	-



736 **LIST OF FIGURES**

737	Fig. 1. Study area of the Ala-Archa basin and Golubin Glacier including the locations of the	
738	water sampling points.....	32
739	Fig. 2. Isotope signatures of water samples from the three seasons in the Ala-Archa	
740	basin	33
741	Fig. 3. $\delta^{18}\text{O}$ -EC mixing space of the various water sources in the three seasons.....	34
742	Fig. 4. Contributions of runoff components to total runoff estimated by different mixing	
743	approaches in three seasons.....	35
744	Fig. 5. Posterior distributions of water tracer signatures estimated by the	
745	Bayesian_4_Cor.....	36
746	Fig. 6. Comparison of the posterior distributions of water tracers estimated by two Bayesian	
747	approaches	37
748	Fig. 7. Correlation between posterior $\delta^{18}\text{O}$ and $\delta^2\text{H}$ estimated by the Bayesian_4_Cor and the	
749	Bayesian_4 approaches	38
750	Fig. 8. Sensitivity of the estimates for the contributions of runoff components to the sampling	
751	uncertainty.....	39
752	Fig. 9. Effects of isotope fractionation on the contributions of runoff components in the	
753	Bayesian approaches.....	40
754	Fig. 10. Effects of isotope fractionation on the posterior distributions of tracer signatures of	
755	water sources in the glacier melt season.....	41

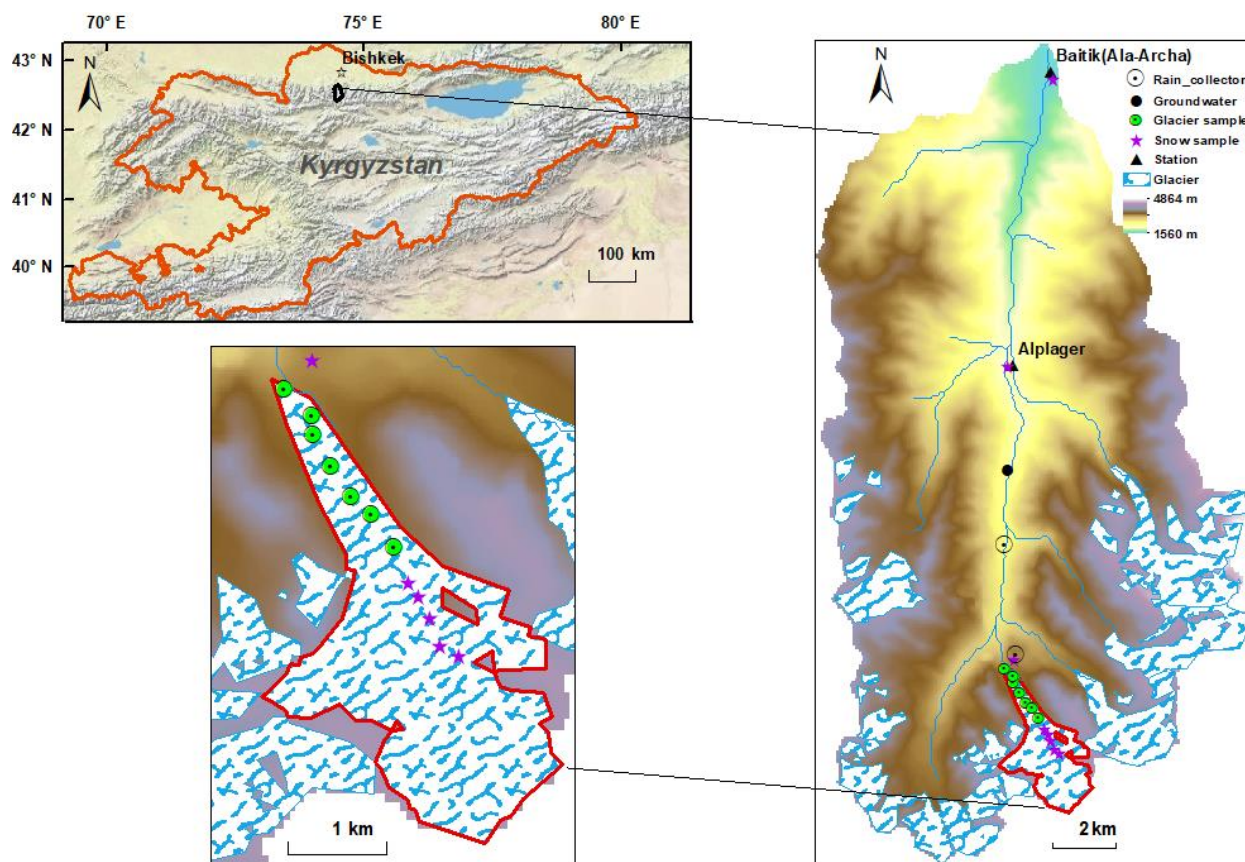
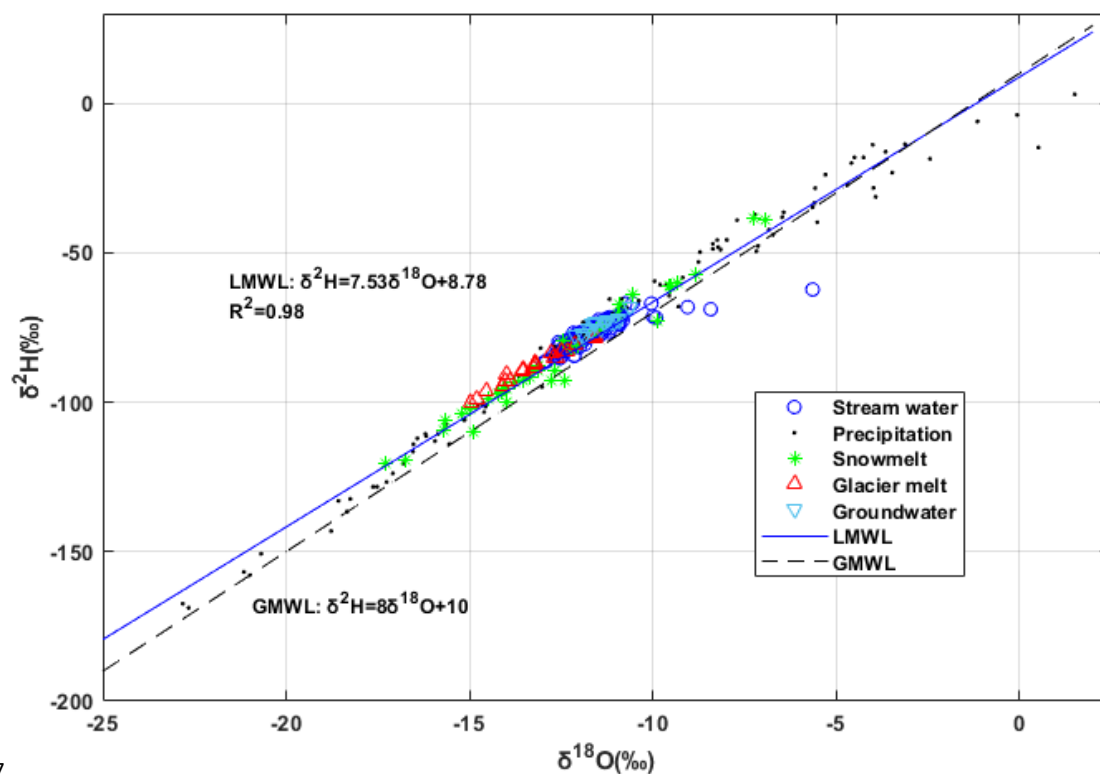


Figure 1. Study area of the Ala-Archa basin (derived from the ESRI World Topographic Map) and the Golubin Glacier including the locations of the water sampling points.



7

760 Figure 2. Isotope signatures of water samples from the three seasons in the Ala-Archa basin.

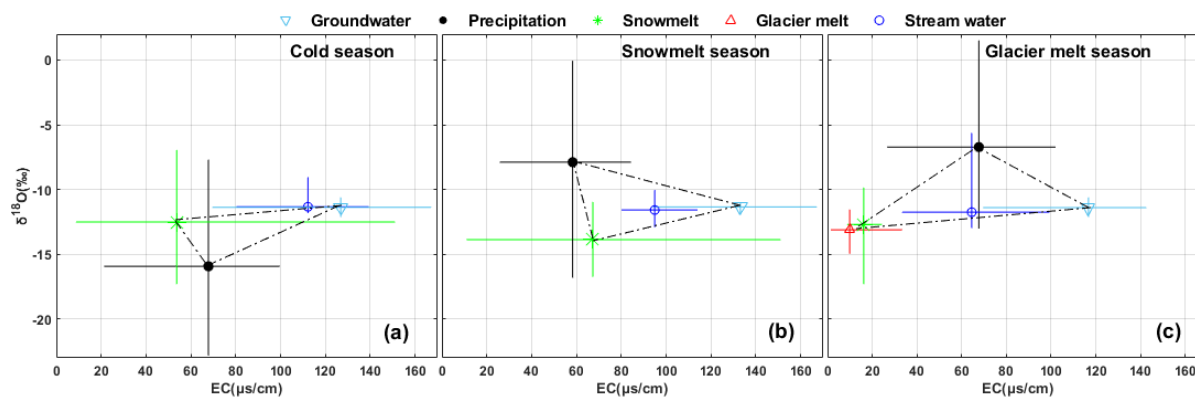


Figure 3. $\delta^{18}\text{O}$ -EC mixing space of the various water sources in the three seasons. The solid lines indicate the ranges of tracer signatures measured from water samples.

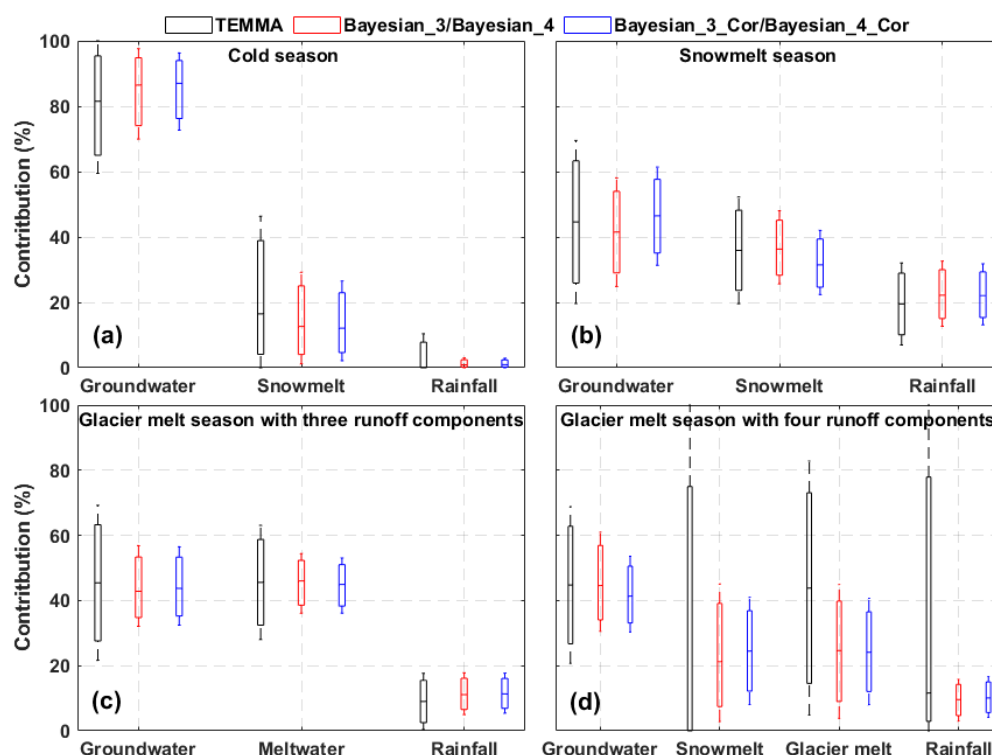
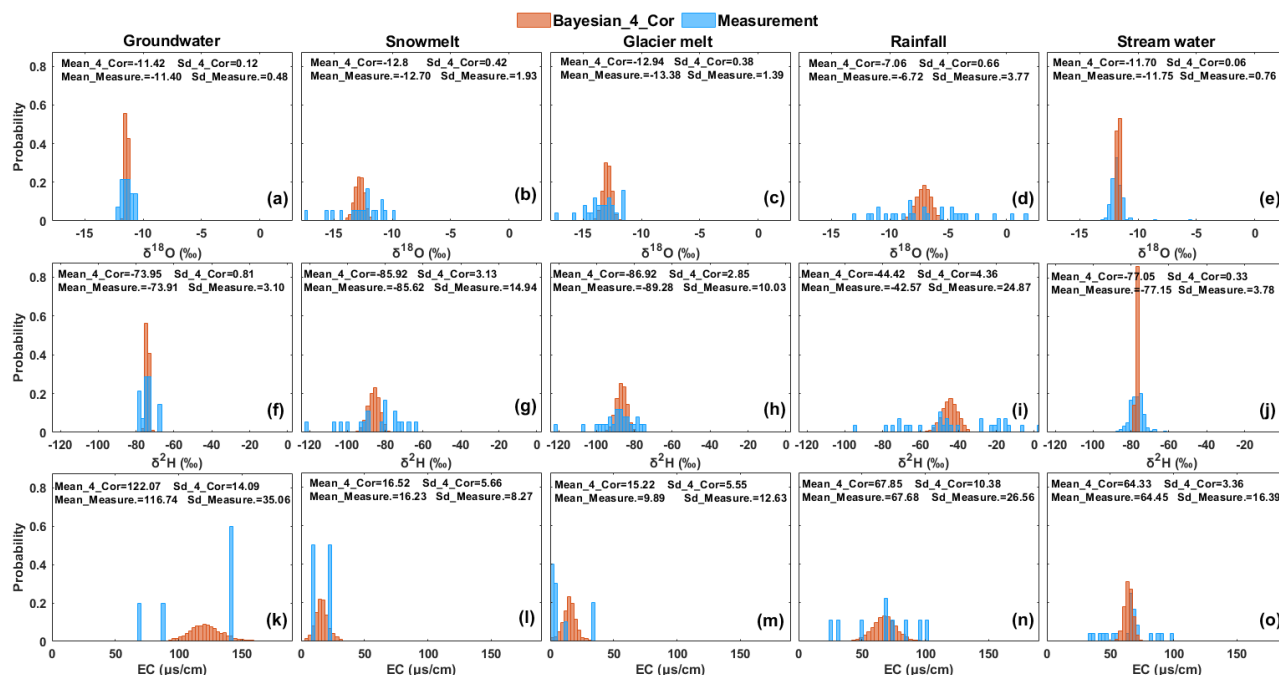
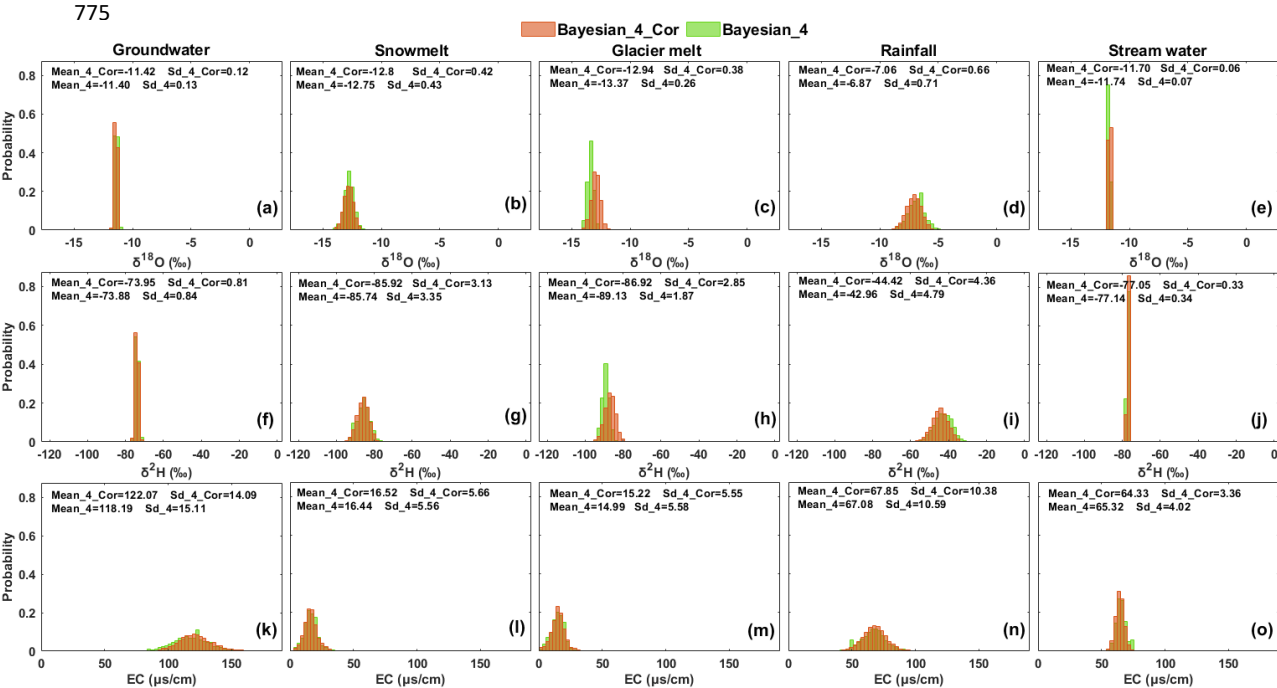


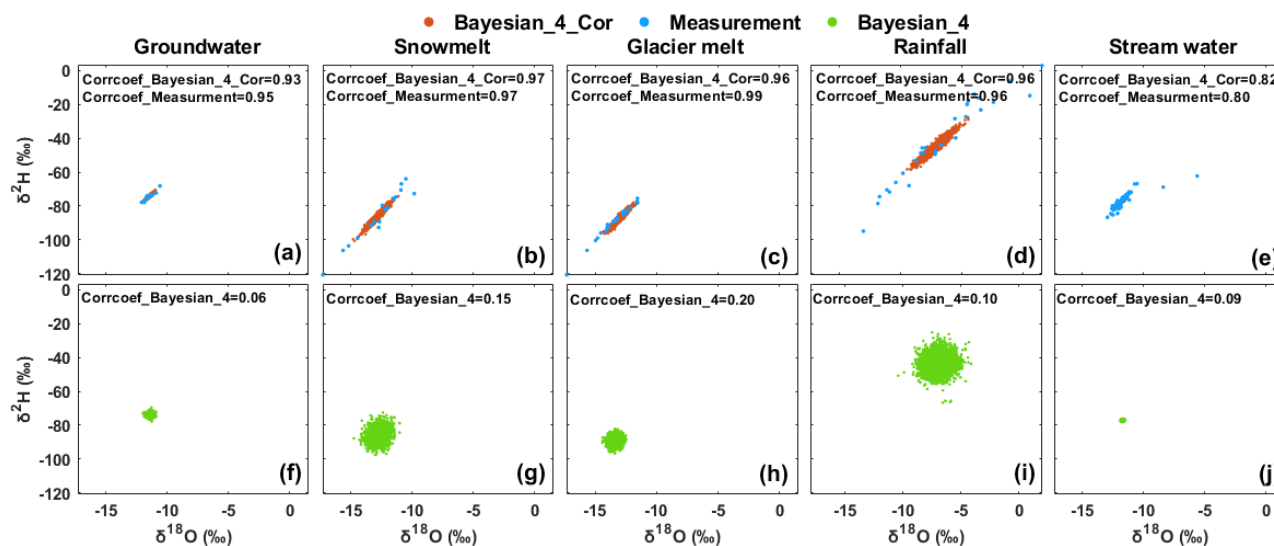
Figure 4. Contributions of runoff components (CRC) to total runoff estimated by different mixing approaches in three seasons. The Bayesian_3 and Bayesian_3_Cor were applied in the cold and melt seasons (a-c), and the Bayesian_4 and Bayesian_4_Cor were applied in the glacier melt season (d). The horizontal lines in the boxes refer to the median contributions, and whiskers refer to the 95% and 5% percentiles.



771 Figure 5. Posterior distributions of water tracer signatures estimated by the Bayesian_4_Cor
 772 in the glacier melt season. Measurement refers to the distributions of water tracer signatures
 773 from the water samples. Row 1: distributions of $\delta^{18}\text{O}$; Row 2: distributions of $\delta^2\text{H}$; Row 3:
 774 distributions of EC.



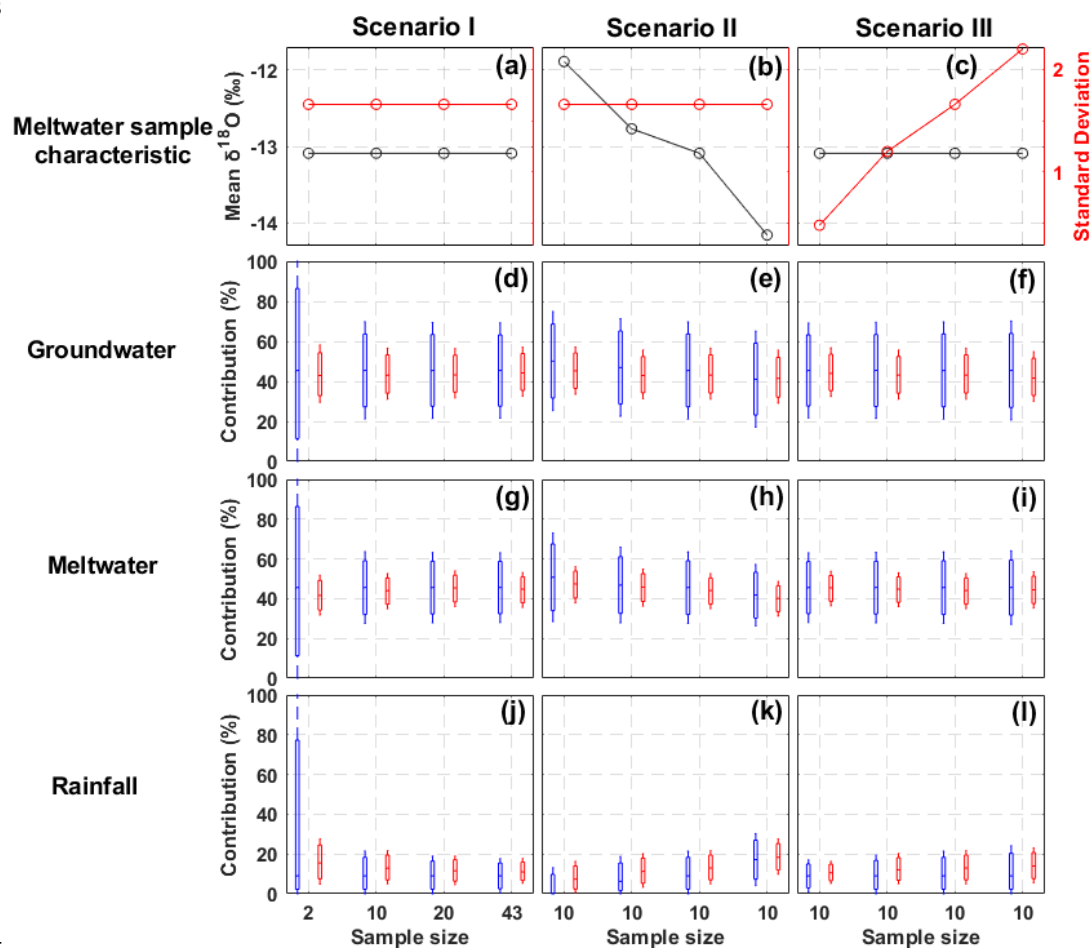
777 Figure 6. Comparison of the posterior distributions of water tracers estimated by the Bayesian
778 approaches with (Bayesian_4_Cor) and without (Bayesian_4) considering the correlation
779 between $\delta^{18}\text{O}$ and $\delta^2\text{H}$ in the glacier melt season.



781 Figure 7. Correlation between posterior $\delta^{18}\text{O}$ and $\delta^2\text{H}$ estimated by the Bayesian_4_Cor and
 782 the Bayesian_4 approaches in the glacier melt season.

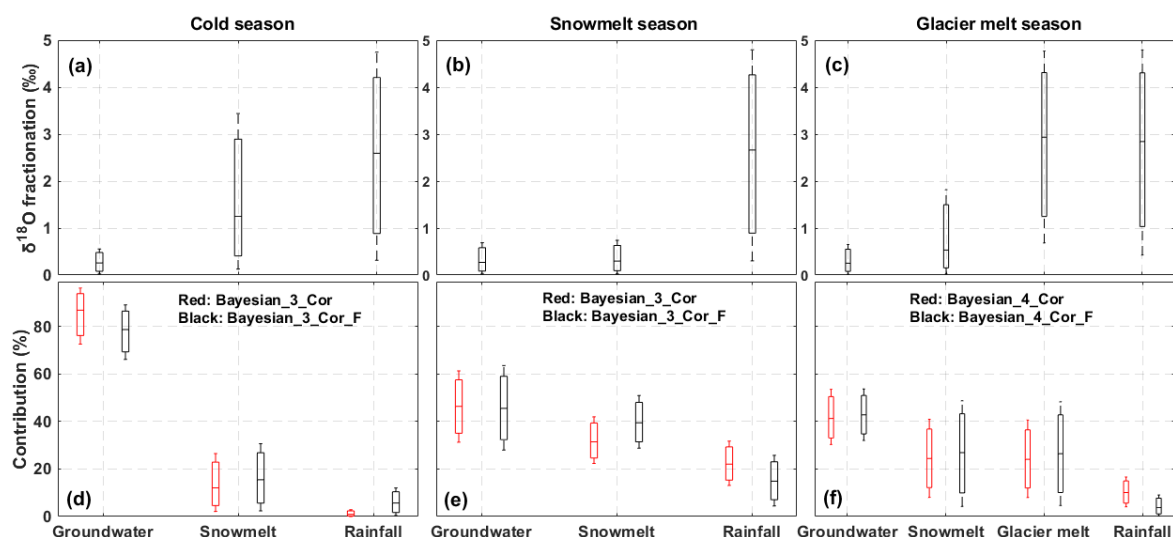


783

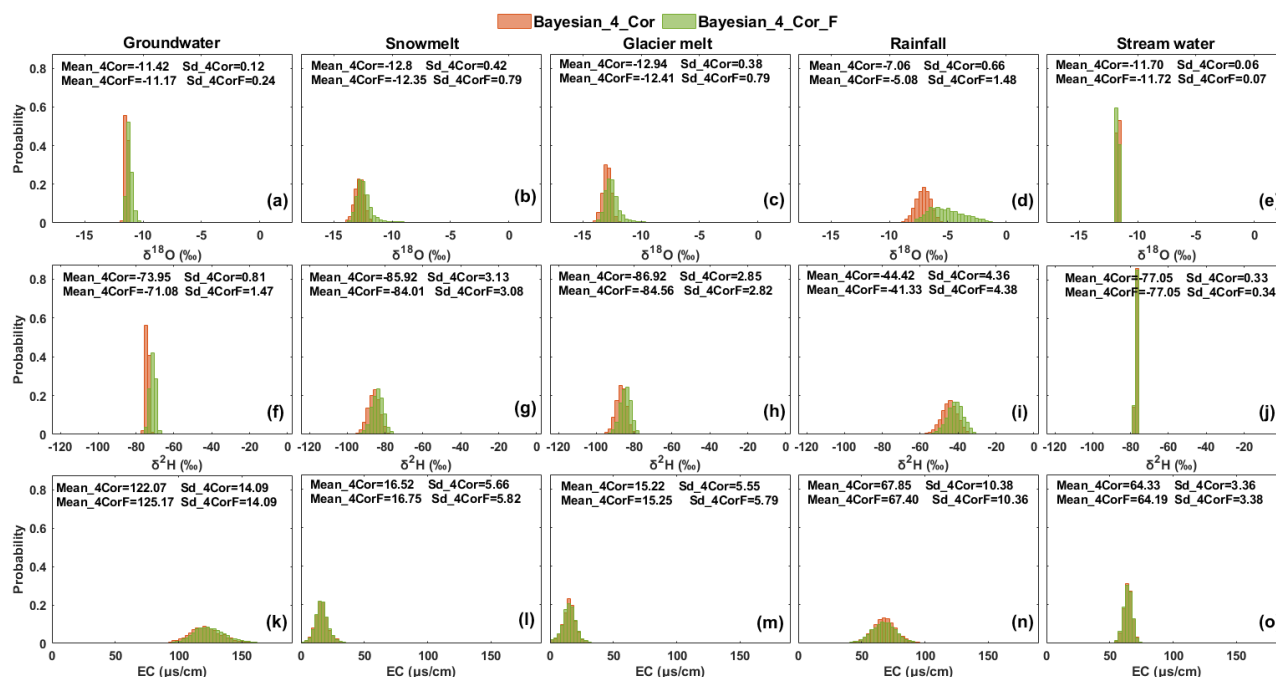


784

785 Figure 8. Sensitivity of the estimates for CRC to the sample size (Scenario I), the mean
 786 (Scenario II) and standard deviation (Scenario III) of $\delta^{18}\text{O}$ of meltwater in the glacier melt
 787 season. Red boxes show the contributions estimated by the Bayesian_3_Cor, and the blue
 788 boxes refer to the contributions estimated by the TEMMA_3.



790 Figure 9. Effects of isotope fractionation on the estimates of CRC in the Bayesian approach
 791 for the three seasons. (a)-(c): Estimated changes in $\delta^{18}\text{O}$ of runoff components caused by the
 792 fractionation effect; (d)-(e): Comparison of the CRC estimated by the Bayesian_3_Cor and
 793 the Bayesian_3_Cor_F; (f): Comparison of the CRC estimated by the Bayesian_4_Cor and
 794 the Bayesian_4_Cor_F.



796 Figure 10. Effects of isotope fractionation on the posterior distributions of tracer signatures of
 797 water sources in the glacier melt season.